

Thermal and mechanical properties of EPDM/PP + thermal shock-resistant ceramic composites

Witold Brostow · Tea Datashvili · James Geodakyan · Jesse Lou

Received: 12 July 2010/Accepted: 16 November 2010/Published online: 9 December 2010
© Springer Science+Business Media, LLC 2010

Abstract Dynamic vulcanizate blends of polypropylene (PP) and ethylene-propylene-diene rubber (EPDM) were filled with 5 wt% of micro-scale ceramic powder. To overcome the difficulty of particles dispersion and adhesion, the filler was modified through grafting using three kinds of organic molecules. A combination of Raman data with thermogravimetric analysis (TGA) results prove that grafting of organic macromolecules onto ceramic surfaces takes place. Dynamic mechanical analysis (DMA) has been performed from –100 to +50 °C; addition of the ceramic increases the storage modulus E' , more so for modified filler. Compared to PP and thermoplastic vulcanizate (TPV), a higher thermal expansion is seen after addition of the ceramic filler, a result of creation of more free volume. The tensile modulus of the composites is about 1.2 times that of pure TPV, an increase in the rigidity clearly caused by the ceramic. Fracture surfaces show weak bonding of filler particles to the matrix. In the sample containing modified filler the tensile deformation is

going through the polymer matrix. The brittleness, B , decreases upon surface modification of the ceramic. The highest value of B is seen for the PP + unmodified ceramic while lower B values are obtained for TPV and its composites.

Introduction

The cost of manufacturing composite structures has proven to be the largest obstacle to their widespread use. The prevailing design and manufacturing approaches rely on assembling large numbers of mechanically fastened parts, a tradition inherited from metallurgy. Affordable composites can be achieved by proper materials selection, using low-cost manufacturing techniques and developing approaches for subsystem integration [1, 2]. Advancements in polymer composites using different fillers, adhesive bonding, and low-cost materials allow designers and manufacturers to exploit well the benefits of these materials [3–6].

Disadvantages of polymer-based composites include complex rheological behavior and difficult fabrication techniques [7–13]. Properties of composite materials are influenced by the properties of the components, shape of the filler, the morphology of the system, and the nature of the interfaces between the phases. A large variety of properties can be obtained with composites just by alteration of one of these items. Interfaces have large influence on the properties of multiphase polymer composites [14–17]. The challenge consists in obtaining significant improvements in the interfacial adhesion between the polymer matrix and the inorganic additives as well as achieving a homogeneous dispersion of the filler in polymer matrix [18–23].

In this work, we have fabricated dynamic vulcanizate blends of polypropylene (PP) with ethylene-propylene-diene

W. Brostow (✉) · T. Datashvili · J. Lou
Laboratory of Advanced Polymers & Optimized Materials (LAPOM), Department of Materials Science and Engineering and Department of Physics, University of North Texas, 1150 Union Circle # 305310, Denton, TX 76203-5017, USA
e-mail: brostow@unt.edu; wbrostow@yahoo.com
URL: <http://www.unt.edu/LAPOM/>

T. Datashvili
e-mail: tcd0033@unt.edu

J. Lou
e-mail: Lou.Jesse@gmail.com

J. Geodakyan
Scientific Research and Production Enterprise of Materials Science, 17 Charents Street, 0025 Yerevan, Armenia
e-mail: JGeodakyan@rambler.ru

rubber (EPDM) [24] filled with 5 wt% of a micro-scale ceramic powder. We have avoided this way a large increase in density—which would introduce an extra factor affecting the properties. EPDM + PP (50 wt% + 50 wt%) compounds were dynamically vulcanized by melt mixing at 190 °C using dicumyl peroxide. To overcome the difficulty of particles dispersion and adhesion to the matrix, the filler was modified through grafting of a polymerizable organic silane and a titanate onto surfaces of ceramic powders via hydroxyl groups. Additionally, stearic acid was used as a third agent for coating the surface of the ceramic filler. The powders were mixed through vulcanization with EPDM + PP.

For comparison, thermal and mechanical properties of unfilled thermoplastic vulcanizate (TPV) and TPV filled with neat powder were also evaluated under identical test conditions.

Experimental part

Materials

The thermal shock-resistant ceramic powder contains corundum (α -Al₂O₃), mullite (3Al₂O₃·2SiO₂), the eutectic of both (a summary formula \approx 2Al₂O₃SiO₂), modified β -spodumene (with negative thermal expansivity) and stabilized aluminum titanate. The composite was prepared by interaction of the minerals in the air atmosphere at 1550 °C temperature for 5 h. Subsequently wet pressing in the presence of water + ethanol was applied in a circular type mill followed by drying. The material has density $\rho = 3.60 \text{ g cm}^{-3}$, open porosity 0.46%, and total porosity 20.0%; the average volumetric thermal expansivity in the large range from 20 to 700 °C is $\alpha = 2.5 \cdot 10^{-6} \text{ K}^{-1}$. The material survives multiple thermal cycling up to at least 1400 °C. Some compositions of such powders have been patented [25, 26].

The coupling agents, namely 3MPS (3-methacryloxypropyltrimethoxysilane, SCA 989) and a titanate coupling agent (neopentyl(diallyl)oxy-tri(dioctyl)phosphato titanate)

(Lica12) were received as gifts from Struktol Company of America and Kenrich Petrochemicals, Inc., respectively. EPDM pellets were received as a gift from Dow Chemical Company. PP pellets were supplied by Huntsman Co. Table 1 provides some information on the coupling agents.

Peroxide, ethanol, and stearic acid were from Sigma Chemicals Co. The reagents were analytically pure and were used as received. Table 1 lists some properties of the coupling agents.

Characterization techniques

Differential scanning calorimetry (DSC)

Differential scanning calorimetry (DSC) measurements were performed on a Perkin Elmer DSC-7 instrument. The DSC technique has been well described by Menard [27], Gedde [28], and Lucas et al. [29]. The temperature range from 10 to 200 °C was covered under a nitrogen atmosphere at 10 °C/min heating and cooling rates.

The melting temperatures, T_m , crystallization temperatures, T_c , and enthalpies of fusion H^f were evaluated on the basis of thermograms. Volumetric degree of the crystallinity, X_c , was calculated as

$$X_c[\%] = 100H^f/H_{PP}^f \quad (1)$$

where $H_{PP}^f = 209 \text{ J/g}$ is the enthalpy of fusion [30] of 100% crystalline PP.

Dynamic mechanical analysis (DMA)

This technique is also well described by Menard [27], Gedde [28], and Lucas et al. [29]. The tests were carried out using a DMA7e apparatus from Perkin Elmer Co. Specimens were analyzed in rectangular form using a three point bending fixture in the temperature T scan mode. The frequency applied was 1.0 Hz. We have recorded the storage (solid-like) modulus E' and $\tan \delta$ as a function of temperature

$$\tan \delta = E''/E' \quad (2)$$

Table 1 The coupling agents

Trade name	Chemical description	Chemical structure	Boiling point/°C
SCA 989	3-Methacryloxypropyltrimethoxysilane	$\text{H}_2\text{C}=\text{C}(\text{CH}_3)\text{CO}_2(\text{CH}_2)_3\text{Si}(\text{OCH}_3)_3$	255
Lica12	Neopentyl(diallyl)oxy-tri(dioctyl)phosphato titanate	$\begin{array}{c} \text{CH}_2=\text{CH}-\text{CH}_2\text{O}-\text{CH}_2 \\ \\ \text{CH}_3\text{CH}_2-\text{C}-\text{CH}_2-\text{O}-\text{Ti}\left(-\text{O}-\text{P}(\text{O})(\text{OC}_8\text{H}_{17})_2\right)_3 \end{array}$	71
Stearic acid	Octadecanoic acid	$\text{C}_{18}\text{H}_{36}\text{O}_2$	383

where E'' is the loss (liquid-like) modulus.

Thermal mechanical analysis (TMA)

This technique has also been discussed in the literature quoted [27–29]. Samples were analyzed in the temperature T scan mode using a DMA7e apparatus from Perkin Elmer Co with a compression analysis kit. The experiments were performed over the temperature range from -50 to $+100$ °C at the heating rate of 10 °C/min. TMA experiments provide values of linear isobaric expansivity (often called thermal expansion coefficient) defined as

$$\alpha_L = L^{-1}(\partial L / \partial T)_P \quad (3)$$

where L is the length (actually height, the distance between top and bottom parallel surfaces) of the sample, T is the temperature, and P is the pressure. The volumetric isobaric expansivity, α , is defined analogously but with the volume V instead of L .

Thermogravimetric analysis (TGA)

A Perkin Elmer TG-7 instrument was used to determine a temperature profile of the powder. 5.0 mg of each dried sample were placed on a balance and heated over the temperature range from $+50$ to 600 °C in nitrogen atmosphere at the heating rate of 10 °C/min.

Raman spectroscopy

Raman spectra of the samples were obtained in the 3000 to 150 cm $^{-1}$ range with a Nicolet Almega XR Dispersive Raman spectrometer. The 780 nm line laser was used as an excitation source. The collecting exposure time, preview exposure time, and sample exposure were 10.0, 0.5, and 10.0 s, respectively.

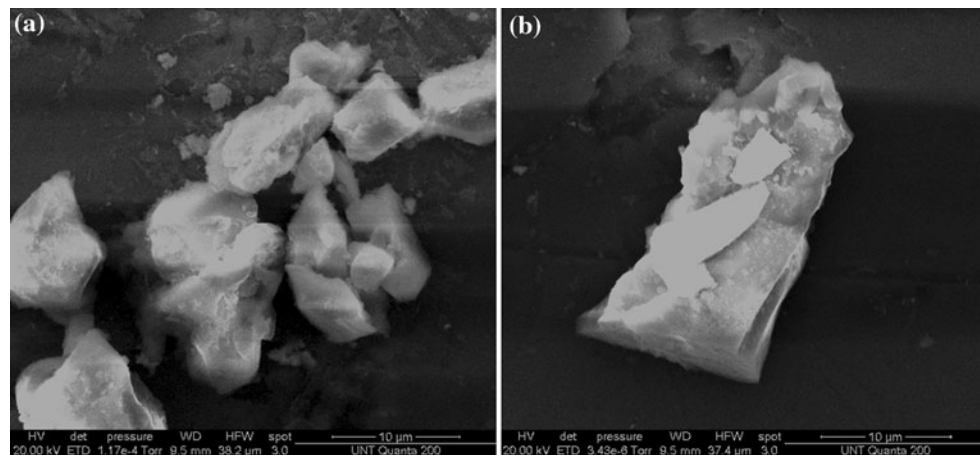


Fig. 1 ESEM images of the ceramic powder

Environmental scanning electron microscopy

Micrographs of all samples were taken using a FEI Quanta environmental scanning electron microscope (ESEM). A small fraction of the samples were cut and/or fractured in liquid nitrogen, mounted each on a copper stub, and coated with a thin layer of gold to avoid electrostatic charging during examination.

Tensile testing

The static tensile behavior of the samples was determined at room temperature (25 °C) with a MTS tester (model QTEST/5). The tests performed in a controlled environment and aimed to determine primarily the strain at break ε_b and the tensile modulus E . The cross-head speed was 100 mm/min; five specimens of each sample were tested and average values are reported.

Characterization of ceramic composite

Ceramic particle shapes and sizes were studied by ESEM. Figure 1 displays an ESEM image of the filler.

We see in Fig. 1 that the particles are not uniform in shape and size. The particles have approximately a rectangular shape; the outer diameter of each varies from 3 to 10 μm, with the length ranging from 10 to 30 μm.

Modification of ceramic particles

Three different types of coupling agents (CAs) were used for modification of the ceramic powder.

At first, 2 wt% CAs solutions in ethanol were prepared. MPS and Lica12 are liquid, but stearic acid is a solid. To make a stearic acid solution, we first melted the acid in a steel pot at 70 °C and then dissolved it in ethanol.

The final reaction mixture contained powder with 2 wt% CA alcohol solution in a 1:5 weight ratio. The solution was added to powder slowly into a mixer with a constant stirring rate at room temperature. The mixing was conducted for 24 h at room temperature.

Afterwards, the powder was centrifuged and washed with fresh alcohol to remove the excess CA absorbed on the surfaces. Final products were dried at 40 °C under a vacuum for 24 h.

Blending and sample preparation

The process of vulcanization was performed by melt mixing in a C.W. Brabender D-52 Preparation Station. EPDM was added first and softened at 160 °C with 60 rpm speed for 2 min, followed by addition of PP. After 2 min of mixing, 5 wt% of powder was added. Immediately afterwards, 1 wt% of the curing agent was added, and temperature and mixing speed were increased and kept for

2 min at 190 °C and 90 rpm. The amount of peroxide was calculated on the basis of the EPDM + PP weight.

Subsequently, the resulting samples were pelletized and the blends were then molded in an AB-100 injection molding machine (AB Machinery, Montreal, Quebec, Canada) at 185 °C with an injection pressure of 830 kPa.

TGA and Raman spectroscopy of the ceramic powder

The principles of surface modification of the ceramic powder are presented schematically in Fig. 2.

Thermal stability of the powders has been investigated by TGA. The resulting diagrams are shown in Fig. 3.

Thermograms of the modified samples show two regions of characteristic weight loss at 200–350 °C and 350–550 °C. Thermal degradation of MPS-modified ceramic powder also occurs in a similar manner; however, the first endotherm appears only around 320 °C and it

Fig. 2 Surface modification of ceramic powders

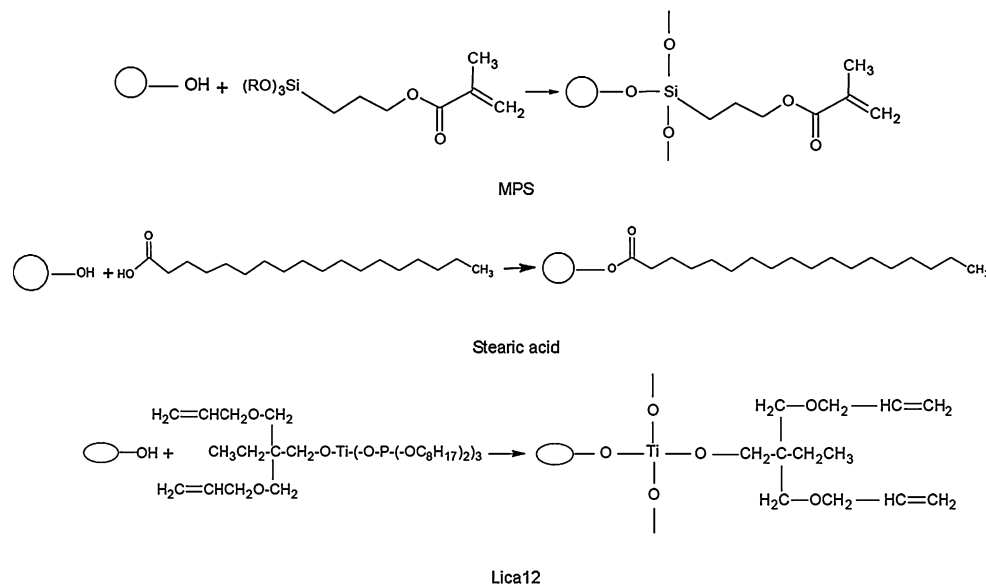
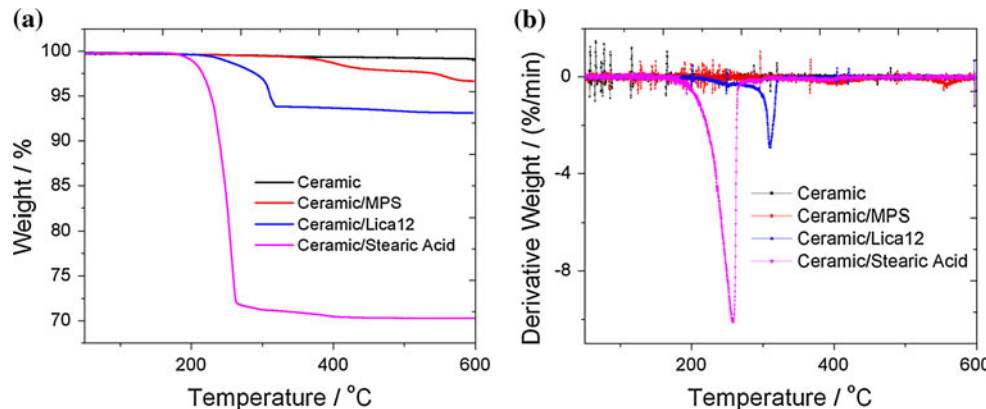


Fig. 3 TGA scans **a** and derivative curves **b** of the ceramic



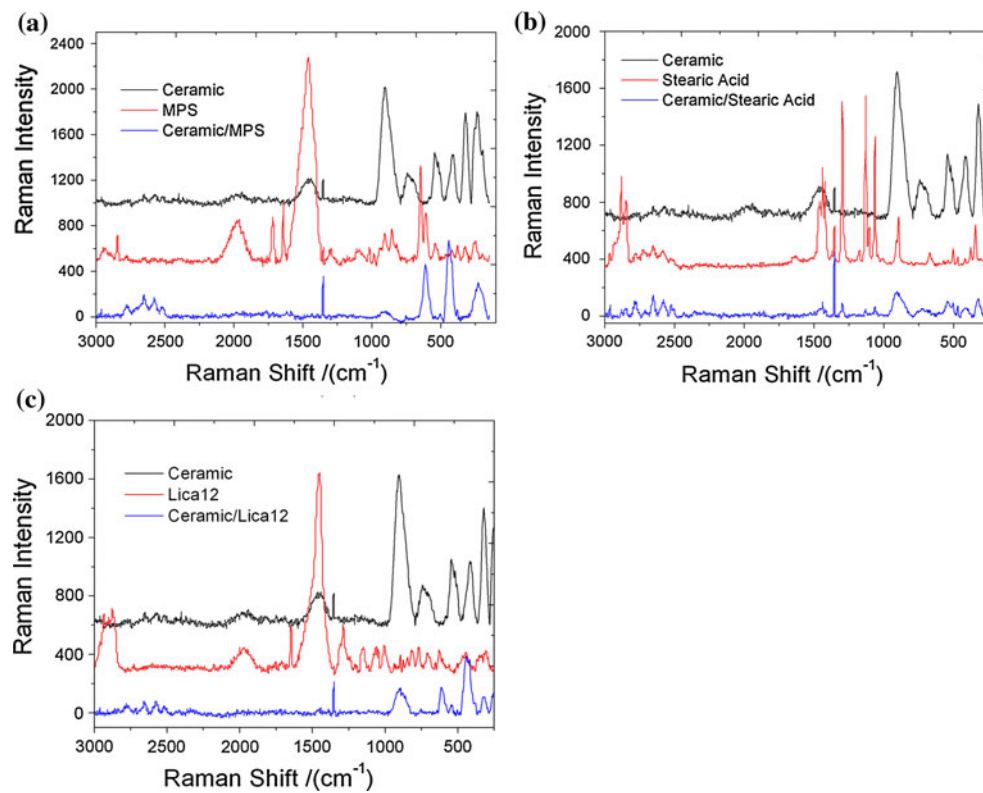
represents a mass loss of ≈ 1.5 wt%. The second step starts at 500 °C and continues until 600 °C. The decomposition below 450 °C can be explained by degradation of the organic constituents of the grafted CA. As we see from Fig. 3b, an endothermic peak above 500 °C is only observed for MPS treated ceramic powder; it represents elimination of residual hydroxyl groups due to densification of SiO₂ network at high temperatures. The weight of the neat powder remains constant even at 600 °C. Significant differences in thermal behavior between the unmodified and modified samples are associated with the organic groups formed through modification on the powder surfaces.

Interactions between CAs and powder surfaces have been also studied by Raman spectroscopy. We recall that the main components of ceramic powder are α -Al₂O₃ and mullite. Hydroxide groups on the ceramic particle surfaces serve for grafting organic macromolecules on them. The attachment of organic molecules to Al₂O₃ is believed to occur in a manner analogous to the attachment of organic molecules to silica. MPS, Lica12, and stearic acid, after reacting with hydroxyls on the Al₂O₃ surface, can form Al–O–Si, Al–O–Ni and Al–O–C bonds, respectively. The surface hydroxyl concentration for porous γ -Al₂O₃ and α -Al₂O₃ surfaces is estimated to be between 2 and 10 hydroxyls/10 nm, depending upon preparation procedure.

Silica has hydroxyl coverage of ≈ 4.5 hydroxyls/10 nm [31]. Therefore, coverages for the molecules attached to Al₂O₃ should be roughly comparable to those on silica.

Figure 4 shows Raman spectra for neat ceramic before and after modification. Recall that one of the molecules used to modify ceramic powder is MPS which contains a methacrylate group. The most important mode for MPS is doublet at 1718 cm⁻¹, assigned to carbonyl ester groups, hydrogen-bonded and non hydrogen-bonded to silanol groups, respectively; the band at 1641 cm⁻¹ is assigned to C=C stretching mode. The Raman bands at 2947, 2844, 1463, 1096 cm⁻¹ are attributed to the OCH₃ group vibrations; the doublet seen at 607 [$\nu(\text{Si}–\text{O}–\text{CH}_3)_3$ anti-symmetric stretching] and 646 cm⁻¹ [$\nu(\text{Si}–\text{O}–\text{CH}_3)_3$ symmetric stretching] can be used to follow the progress of the grafting reaction. The Raman spectra of the ceramic with MPS show disappearance of the methoxy bands at 2844 and 825 cm⁻¹ as a result of hydrolysis. Another evidence of grafting reaction progress is provided by appearance of bands in the 2500–3000 cm⁻¹ that is $\nu(\text{C}–\text{H})$ region, corresponding to characteristic bands of organic molecules: $\nu_s(\text{CH}_2)$, $\nu_a(\text{CH}_2)$, and $\nu_s(=\text{CH}_2)$. The spectra also show the presence of weak bands near 1590 and 505 cm⁻¹, probably contributed by Si–O–Al and Si–O–Si vibrations, respectively. These results suggest that the MPS macromolecules are bonded to ceramic surface.

Fig. 4 Raman spectra of the powder with MPS (a), stearic acid (b), and Lica12 (c)



Let us consider now the powder modification process with stearic acid. In Fig. 4b, we see characteristic Raman bands for the stearic acid at 1064, 1130, 1296 cm^{-1} and a group of bands in 1400–1500 cm^{-1} region due to $\nu(\text{C}-\text{C})$ stretching vibrations, (CH_2) twist vibrations, and $\delta(\text{CH}_3)$ or $\delta(\text{CH}_2)$ deformations, respectively. Raman spectra of the ceramic powder treated with stearic acid show weak $\nu(\text{C}-\text{C})$ bands at 1064 cm^{-1} and 1130 cm^{-1} , CH_2 twist near 1296 cm^{-1} and $\text{CH}_2 \text{ rk}_{\text{G}}$ modes at 892 and 687 cm^{-1} . The vibration associated with the $\nu(\text{C}-\text{C})_{\text{G}}$ conformation appears as a very weak signal around 1100 cm^{-1} . The intensities of the bands suggest that the carbon backbone of stearic acid is largely in the *trans* conformation. This conclusion is consistent with Raman spectroscopy results of Moskovits and Suh [30] and Thompson and Pemberton [32].

The third CA used to modify ceramic surface was Neopentyl(diallyl)oxytri(dioctyl)phosphato titanate. Characteristic Raman vibrations of Lica12 and the modified powder are seen in Fig. 4c. The spectrum of Lica12 shows strong bands at 1456 and 1647 cm^{-1} corresponding to the $\delta(\text{COH})$ and $\nu(\text{C}=\text{C})$ vibrations, respectively. Other distinctive signals at 1288 cm^{-1} and below are assigned to the $\delta(\text{C}-\text{O})$, $\delta(\text{CH}_2)$, $\nu(\text{Ti}-\text{O}-\text{C})$, $\nu(\text{Ti}-\text{O})$ groups, while $\nu_s(\text{CH}_3)$, $\nu_{\text{as}}(\text{CH}_2)$, and $\nu_s(\text{CH}_2)$ bands are located in the 2800–2980 cm^{-1} range.

Compared to the neat ceramic, the Raman spectra of ceramic powder + Lica12 feature new bands around 360 and 467 cm^{-1} . These signals can be assigned to symmetric stretching vibrations of $\nu(\text{Si}-\text{O}-\text{Ti})$, $\nu(\text{Al}-\text{O}-\text{Ti})$, $\nu(\text{Ti}-\text{O}-\text{Ti})$, or $\nu(\text{xmetal-0})$ [33]. Traces of the asymmetric vibrations can be seen between 1000 and 1100 cm^{-1} range; however, the signals are very weak and their location is difficult. Another evidence of ceramic treatment is the presence of shoulders between 2500 and 3000 cm^{-1} which are related to $\nu(\text{C}-\text{H})$ vibrations.

A combination of Raman data with our TGA results proves ceramic surface modification; apparently grafting

organic macromolecules onto ceramic surface has taken place.

Dynamic and thermophysical properties

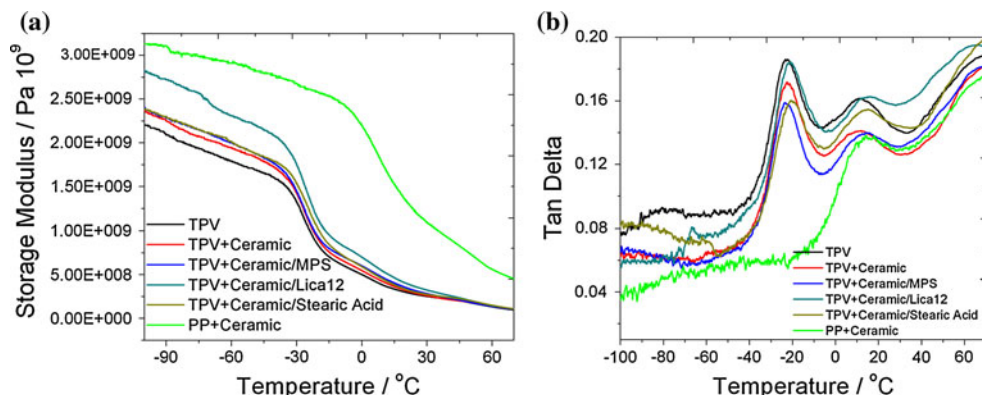
We begin with DMA results. Figure 5a, b displays, respectively, the storage modulus E' and $\tan\delta$ diagrams as a function of temperature.

Two separate transitions from a glassy to a rubbery state are visible in the temperature range from -100 to $+50$ $^{\circ}\text{C}$; they correspond to relaxations of the individual components. For each sample, the peak at the lower temperature is the glass transition temperature of the elastomer whereas the peak at the higher temperature is that of PP. Two distinct peaks nearly independent of temperature indicate the immiscibility between the EPDM and PP components. The issue of miscibility, compatibility, and immiscibility has been discussed in earlier papers [34–36].

Incorporation of ceramic fillers—modified or otherwise—into the polymer matrix increases the storage E' modulae values in the entire temperature range studied, from -100 to $+50$ $^{\circ}\text{C}$. Powder fillers are known to increase also the viscosity of melts [37]. Modulae of all TPV composites containing surface modified ceramics are higher than for the TPV + ceramic without CA. This indicates that the interaction between the filler and TPV has increased after modification.

The glass transition temperatures T_g values can be located either as the midpoint of the descent of E' or else as peaks of $\tan\delta$ [35]. In either case, we see that T_g values are only insignificantly affected by the presence of the ceramic or its modification. One can notice a small broadening of the $\tan\delta$ peaks around the glass transition. A possible explanation is that the unconstrained segments of the polymer retain the glass transition temperatures of bulk TPV while those segments in the vicinity of the filler are less mobile and slightly shift T_g upwards. Small as this

Fig. 5 DMA results: storage modulus E' (a) and $\tan\delta$ (b)



effect is, it is slightly larger for the composites with CA—a consequence of improved adhesion between the ceramic particles and the TPV matrix.

Linear isobaric expansivities were calculated from TMA results according to Eq. 3. As we know, T_g in a polymer corresponds to expansion of the free volume allowing greater chain mobility above this transition. From DMA and TMA curves we see that the T_g transitions are located in the temperature range from -40 to $+40$ °C. We have determined the dimensional changes of the samples below and above T_g . The average values of α_L for the range from -60 to -40 °C and 40 to 90 °C are presented in Fig. 6.

As expected, below T_g all the samples have lower expansivities than above T_g ; at low temperatures chain vibrations are frozen by increased stiffness of C–C bonds and allowing only limited motions of the chain as a whole. α_L of TPV above T_g is $243 \cdot 10^{-6}$ K $^{-1}$ while PP has $68 \cdot 10^{-6}$ K $^{-1}$. Expansivity of the ceramic powder is $2.5 \cdot 10^{-6}$ K $^{-1}$ much less than α_L of our polymeric materials. However, in comparison with PP and TPV, higher expansivity was observed after addition of the filler to each polymeric matrix. This can be attributed to a disruption of the polymer cohesion caused by the ceramic powder. For any material, whether a neat polymer or a composite, free volume can be represented [38, 39] as

$$v^f = v - v^* \quad (4)$$

Here all quantities pertain to a unit mass such as 1 g, v is the specific volume while v^* is the hard-core (incompressible) volume. Apparently free volume v^f is higher in the presence of a ceramic.

We now consider the thermal expansivity behavior of composites with various CAs. We find that the dimensional response with temperature changes in a different manner than for the unmodified ceramics. Apparently some other factors are at play here. A temperature, T , increase affects transmission of stress across interfaces and is thus related to adhesion between the phases. When we heat unmodified composites, the matrix expansion is higher than that of the particles; because of poor adhesion between the two phases, there are no residual compressive stresses across the

interface. As a result, the matrix expands away from the particles. CAs cause more “cooperation” of the filler with the matrix; actually filler particles hinder somewhat the matrix expansion. Hence in Fig. 6b lower expansivities of TVP + MPS-modified ceramic and of TVP + Lica12-modified ceramic. Modification of the filler with stearic acid has a negligible effect.

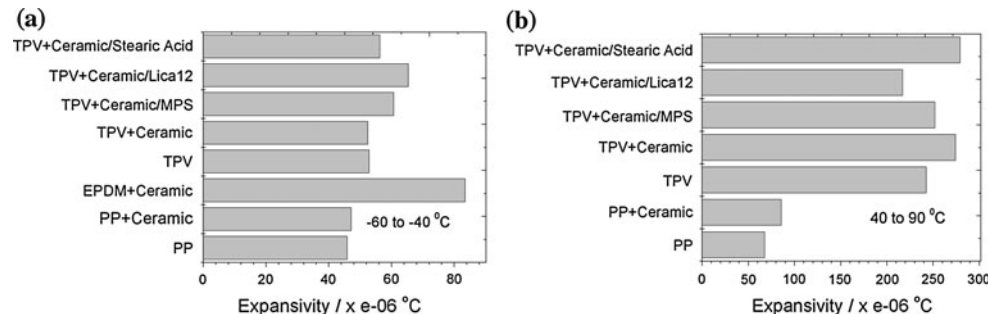
Given potential applications of polymers and polymer-based hybrids for encapsulation of thermoelectric materials, important is avoidance of mismatch of α_L values in TE devices. A wide range of expansivity values seen in Fig. 6b suggest that approximate matching of expansivity values of materials used in such devices should be doable.

Differential scanning calorimetry (DSC) analysis was performed in order to assess possible changes in the crystalline structure and overall crystallization behavior of the polymer matrix. From the recorded melting and crystallization patterns, the thermal parameters such as crystallization temperature, T_c , melting temperature, T_m , the enthalpy of crystallization, H^f , and the degree of crystallinity, X_c , values (see again Eq. 1) were obtained. DSC diagrams are presented in Fig. 7.

Differential scanning calorimetry (DSC) curves clearly demonstrate that the addition of the filler increases the crystallization temperature. For PP + ceramic the increase is from 83.6 to 89.3 °C. By contrast, addition of the filler to TPV caused only a small increase of 2 °C. This can be explained by the assumption that in the case of the TPV materials, the ceramic fillers do not act as nucleation sites—in contrast to the PP matrix. Crystallization of PP + ceramic remained almost the same while TPV crystallization was found to be 5% less after introducing ceramic filler in the vulcanization process. Thermal behavior of TPV composites can be understood as a result of decreased PP chain mobility due to increased viscosity of the blends.

As for the melting temperatures of our samples, the melting peaks are located in the 140 – 147 °C temperature range. The addition of the filler to the polymer matrix slightly decreases the melting point. Filler modification—or otherwise—has no significant effect. Thermal characterization parameters are listed in Table 2.

Fig. 6 TMA data



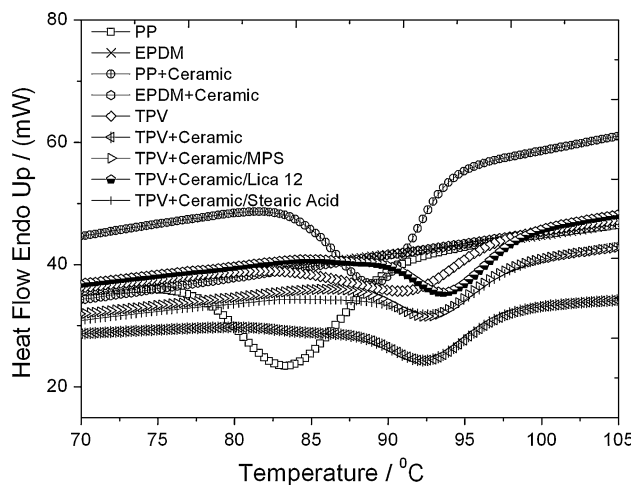


Fig. 7 The DSC cooling thermograms

Table 2 Characterization of the blends

Samples name	$T_g/^\circ\text{C}$	$T_m/^\circ\text{C}$	$H^f/(\text{J g}^{-1})$	$X_c/\%$
PP	83.6	147.0	70.6	33.8
PP + ceramic	89.3	144.7	68.2	32.4
TPV	91.3	144.7	39.4	18.8
TPV + ceramic	92.6	141.7	30.1	14.4
TPV + ceramic/MPS	92.6	144.3	32.9	15.7
TPV + ceramic/Lica12	93.9	140.0	32.5	15.5
TPV + ceramic/stearic acid	92.9	146.3	33.1	15.8

Tensile behavior and brittleness

Figure 8 shows the tensile modulus, E , values at 25 °C. Given the elastomeric nature of EPDM [24], this material has a very low modulus, even after addition of the ceramic. Compared to EPDM, PP is a rigid polymer; addition of the ceramic results in the highest value of E by far among all materials investigated.

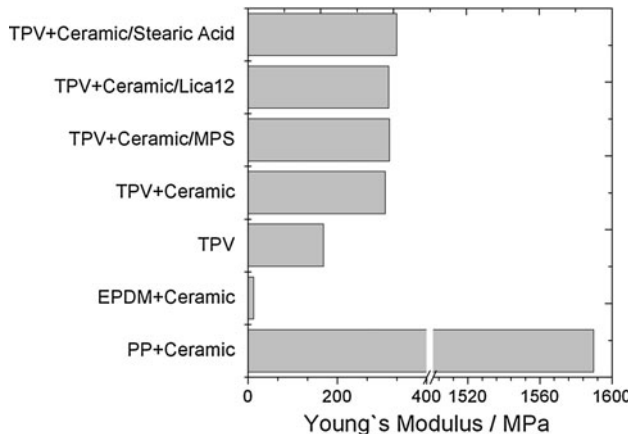


Fig. 8 Young's modulus

As expected, addition of the ceramic to TVP results in the modulus increase. The respective E values are approximately double as compared to neat TPV. Ceramic particles in the matrix hinder movement of the polymeric chains around filler particles, contributing to an overall increase in the modulus. Young's moduli of the composites are somewhat—but not substantially—higher with the modified powders than for the unmodified ceramic. Again we have better cooperation of the filler with the matrix caused by filler modification.

In Fig. 9, we present values of the strain at break, ε_b . As expected, the elastomeric EPDM has by far the highest ε_b , 5 wt%, of the filler notwithstanding. PP with the filler has the lowest value. Effects of the filler on the strain at break of TVP are interesting. The addition of the unmodified ceramic lowers ε_b , apparently a consequence of perturbation of cohesion in the neat polymer by the filler. For modified ceramics, ε_b values are all higher than for neat TPV; once more what we have called improved cooperation of the matrix with the filler is at play.

We know that morphology of the fracture surfaces depends on the interfacial structure due to load transfer between the particles and the polymer matrix. In order to explain the obtained ε_b trends and to evaluate further the role of surface treatment on the deformation processes, ESEM examinations of the fractured surfaces were conducted after tensile testing. Figure 10 displays the ESEM micrographs of the composites.

Environmental scanning electronic microscope (ESEM) images show differences between morphologies of the samples. Neat TPV presents a “plain” surface while fibers are found on the surfaces of the composites after tensile deformation. When the filler is absent, a high shear stress could deform the TPV phase without fibrils formation. The fiber formation process is more pronounced for the composites filled with surface modified powder; the presence of treated fillers induces *longer* fibrils. Moreover, more

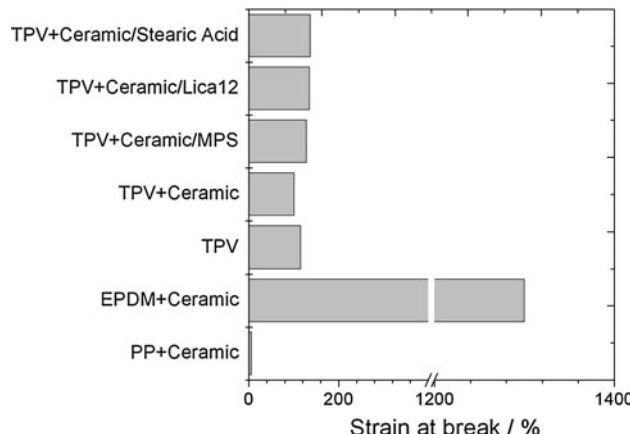


Fig. 9 Strain at break

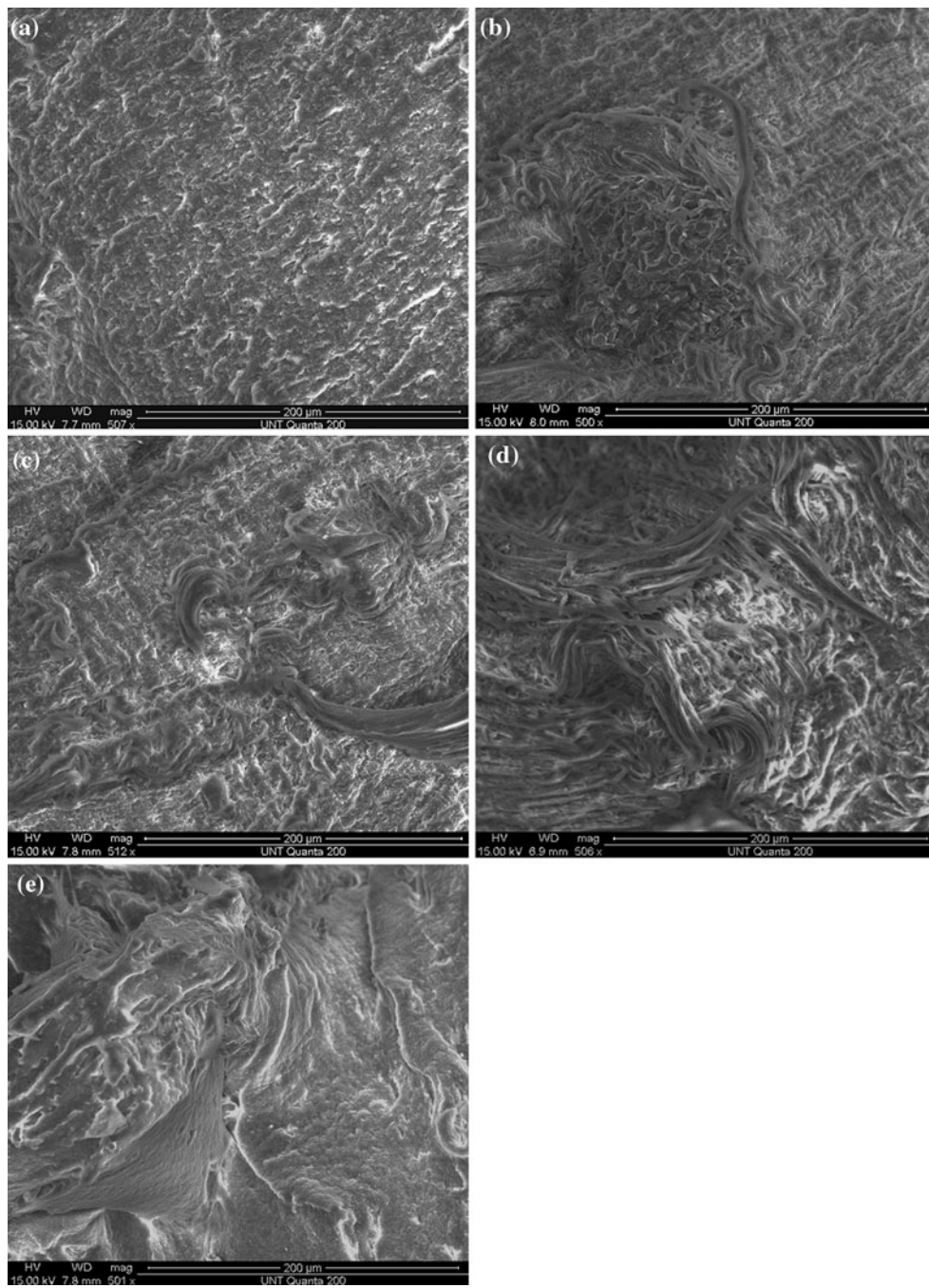


Fig. 10 ESEM micrographs: TPV (a), TPV + ceramic (b), TPV + ceramic/MPS (c), TPV + ceramic/Lica12 (d), TPV + ceramic/stearic acid (e)

numerous fibers are seen in the composite containing Lica12 as compared to that with MPS. This agrees with the fact that ε_b is higher for the composite made using Lica12 than for that with MPS. Extensive fibril formation at the fracture surface indicates improved adhesion between the phases; these facts are consistent with the mechanical behavior discussed above. In all cases, wetting of the particles by the polymer matrix is clearly improved after

coupling treatment, making the interface between two phases almost indistinguishable. The enhancement of the interface can be explained by a decrease in surface energy of the filler after modification; this leads to improvement of compatibility between the phases [14].

Figure 11 shows more detailed views of interfaces between TPV and ceramic particles. After tensile fracture, there is no evidence of adhesion between the unmodified

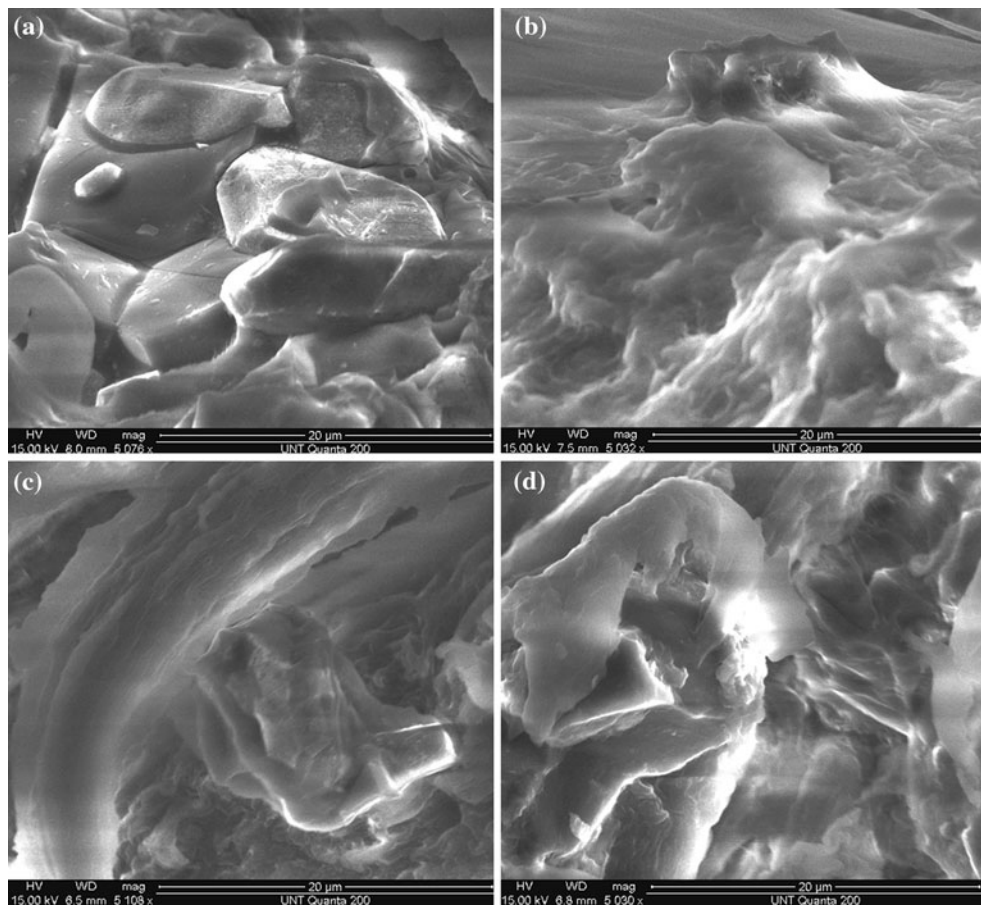


Fig. 11 ESEM micrographs: TPV + ceramic (**a**), TPV + ceramic/MPS (**b**), TPV + ceramic/Lica12 (**c**), TPV + ceramic/stearic acid (**d**)

particles and the polymer matrix; a gap between the two phases is clearly noticeable in high magnification images. Moreover, the fractured surface of TPV + ceramic clearly shows debonding between the filler particle surfaces and the matrix. The possible reason is a lack of adhesion caused by the difference in surface tension and polarity between untreated particles and TPV.

Fractured surfaces of the samples with modified fillers can be seen in Fig. 11b–d. We infer from these micrographs that the coupling agents favor better polymer–filler interactions. The effect is due to replacement of hydroxide groups on surfaces of ceramic oxide powders by organic groups. The sample filled with MPS-modified particles shows that the tensile deformation is going through the polymer matrix; a polymer layer remains on the surface of the particles after tensile testing. A slightly different microstructure is observed for the sample with stearic acid; there is improved interaction between the materials but slight polymer debonding can be observed on the ceramic surface after tensile testing. The micrograph of TPV + ceramic/Lica12 (Fig. 11c) indicates less cohesion between the ceramic surface and the polymer matrix. However, compared to the TPV + unmodified ceramic composite,

the separation between the particle interfaces and the TPV matrix is less pronounced for the modified samples.

We now recall the definition of material brittleness, B [40–42]:

$$B = 1/(E' \varepsilon_b) \quad (5)$$

We have calculated B from results reported above. The values so obtained are displayed in Fig. 12.

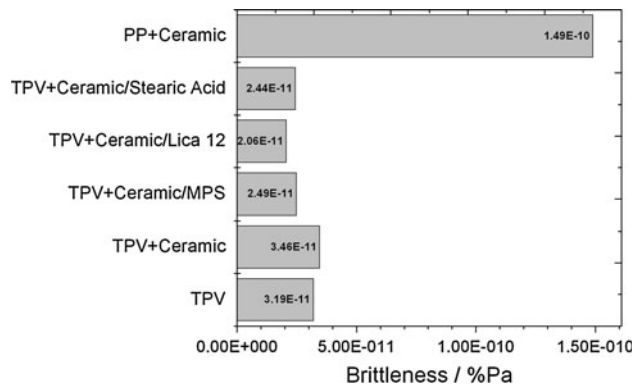


Fig. 12 Brittleness of materials studied

The highest value of brittleness, B , by far is seen for the PP + unmodified ceramic blend. Lower brittleness values are seen for TPV and its composites. Among those composites, surface modification of the ceramic causes B lowering—one more manifestation of what we have called increased cooperation of the matrix with the filler. TPV + ceramic prepared with Lica12 shows the lowest B . Higher strain at break and low brittleness of this composite suggests something akin to plasticization provided by the Lica12 coupling agent. We recall that Chen et al. [43] have demonstrated that improved adhesion between phases causes lowering of brittleness.

Acknowledgements Texas Academy of Mathematics and Science (TAMS), Denton, has provided a research fellowship to one of us (J.L.). Final stages of this project have also been supported by the II-VI Foundation, Bridgeville, PA.

References

- Friedrich K, Lu Z, Hager AM (1995) Wear 190:139
- Pisanova E, Zhandarov S (2000) In: Brostow W (ed) Performance of plastics. Hanser, Munich, Cincinnati
- Castaño VM, Rodriguez JR (2000) In: Brostow W (ed) Performance of plastics. Hanser, Munich, Cincinnati
- Jacob M, Thomas S, Varughese KT (2004) J Compos Sci Technol 64:955
- Sombatsompop N, Thongsang S, Markpin T, Wimolmala E (2004) J Appl Polym Sci 93:2119
- Menon ARR, Sonia TA, Sudha JD (2006) J Appl Polym Sci 102:4801
- Brostow W (ed) (2000) Performance of plastics. Hanser, Munich, Cincinnati
- Brostow W, Deborde J-L, Jaklewicz M, Olszynski P (2003) J Mater Educ 24:119
- Bermudez MD, Brostow W, Carrion-Vilches FJ, Cervantes JJ, Pietkiewicz D (2005) e-Polymers 001:1
- El-Tayeb NSM, Yousif BF (2007) Int J Wear 262:1140
- Stuart BH (1998) Tribol Int 31:647
- Blaszcak P, Brostow W, Datashvili T, Hagg Lobland HE (2010) Polym Compos 31:1913
- Briscoe BJ, Yao LH, Stolarski TA (1986) Wear 108:357
- Kopczynska A, Ehrenstein GW (2007) J Mater Educ 29:325
- Laborie M-PG, Frazier CE (2010) J Mater Sci 41:6001. doi: [10.1007/s10853-006-0497-6](https://doi.org/10.1007/s10853-006-0497-6)
- Bussu G, Lazzeri G (2010) J Mater Sci 41:6072. doi: [10.1007/s10853-006-0694-3](https://doi.org/10.1007/s10853-006-0694-3)
- Mallick K, Witcomb MJ, Scurell MS (2010) J Mater Sci 41:6189. doi: [10.1007/s10853-006-0019-6](https://doi.org/10.1007/s10853-006-0019-6)
- Shanmugharaj AM, Kim JK, Ryu SH (2007) J Appl Polym Sci 104:2237
- Wool RP (2000) In: Brostow W (ed) Performance of plastics. Hanser, Munich, Cincinnati
- Coran AY (1987) In: Bhowmick AK, Stephens HL (eds) Handbook of elastomers—new developments and technology. Marcel Dekker, New York
- Ho RM, Wu CH, Su AC (1990) Polym Eng Sci 30:511
- Jang NZ, Uhlmann DR, Vander Sande JB (1984) J Appl Polym Sci 29:4377
- Montoya M, Tomba JP, Carella JM, Gobernado-Mitre MI (2004) Eur Polym J 40:2757
- Brostow W, Datashvili T, Strate GW, Lohse JD (2009) In: Mark JE (ed) Polymer data handbook, 2nd edn. Oxford University Press, NY, USA
- Geodakyan J, e.a. (2007) Armenian Patent # 1961
- Geodakyan J, e.a. (2007) Armenian Patent # 1962
- Menard KP (2000) In: Brostow W (ed) Performance of plastics. Hanser, Munich, Cincinnati
- Gedde UW (2001) Polymer physics. Springer-Kluver, Dordrecht, Boston
- Lucas EF, Soares BG, Monteiro E (2001) Caracterização de polímeros, e-papers, Rio de Janeiro
- Mandelkern L, Alamo RG (1996) In: Mark JE (ed) Physical properties of polymers handbook. AIP Press, Woodbury, New York
- Moskovits M, Suh JS (1985) J Am Chem Soc 107:6826
- Thompson WR, Pemberton JE (1995) Langmuir 11:1720
- Smith E, Dent G (2005) Modern Raman spectroscopy: a practical approach. John Wiley & Sons, London
- Brostow W, Chiu R, Kalogeras IM, Vassilikou-Dova A (2008) Mater Lett 62:3152
- Brostow W, Deshpande S, Pietkiewicz D, Wisner SR (2009) e-Polymers 109:1
- Babu RJ, Brostow W, Kalogeras I, Sathigari S (2009) Mater Lett 63:2666
- Vu YT, Mark JE, Pham LH, Engelhardt M (2001) J Appl Polym Sci 82:1391
- Flory PJ (1985) Selected works, vol 3. Stanford University Press, Stanford, CA, USA
- Brostow W (2009) Pure Appl Chem 81:417
- Brostow W, Hagg Lobland HE, Narkis M (2006) J Mater Res 21:2422
- Brostow W, Hagg Lobland HE (2008) Polym Eng Sci 49:1985
- Brostow W, Hagg Lobland HE (2010) J Mater Sci 45:242. doi: [10.1007/s10853-009-3926-5](https://doi.org/10.1007/s10853-009-3926-5)
- Chen J, Wang M, Li J, Guo S, Xu S, Zhang Y, Li T, Wen M (2009) Eur Polym J 45:3269